Received: Added at production | Revised: Added at production | Accepted: Added at production

DOI: xxx/xxxx

RESEARCH ARTICLE

Adaptive FEM-validated surrogate optimization of buckling-delayed shear-link dampers for seismic damage mitigation

J. Irazabal[1] | **J. Ramirez**[1,2] | **J. M. Gonzalez**[1,2] | **L. Lazaro**[1] | **F. Rastellini**[1,2] | **G. Bozzo**[2,3] | **L. Bozzo**[4]

[1]Centre Internacional de Metodes Numerics en Enginyeria (CIMNE), Barcelona, Spain

[2]Universitat Politecnica de Catalunya (UPC), Barcelona, Spain

[3]SLB Devices, Barcelona, Spain

[4]Luis Bozzo Estructuras y Proyectos S.L., Barcelona, Spain

Correspondence
J. Irazabal.
Email: jirazabal@cimne.upc.edu

Abstract

Buckling-delayed shear-link (BDSL) dampers are extensively used in seismic-resistant structures as passive devices that concentrate energy dissipation while limiting damage to the primary system. Their geometric optimization requires a compromise between high energy dissipation and control of local damage. Finite element method (FEM) models can reproduce with high accuracy the nonlinear cyclic response of these devices and provide internal quantities such as damage indicators and local distortion but their computational cost prevents their direct use inside iterative optimization loops. This work proposes an adaptive surrogate-assisted optimization framework for BDSL dampers. First, experimentally calibrated nonlinear FEM models are used to generate ground-truth datasets for damper configurations with different numbers of windows and geometric proportions. Supervised learning models are first evaluated, where Support Vector Regression (SVR) and Gaussian Process Regression (GPR)—both based on radial kernel functions—consistently provide the highest predictive accuracy. Motivated by this observation, Radial Basis Function (RBF) surrogates are subsequently introduced as a computationally efficient alternative. The surrogate predictions are coupled with a Differential Evolution algorithm through a damage-aware objective function that limits the damage and uses dissipated energy as a tie-breaking performance criterion. In addition, SHapley Additive exPlanations (SHAP) are employed to quantify the influence of window thickness on damage distribution, with particular emphasis on the response of the surrounding frame. Optimized geometries are finally re-evaluated with FEM. When the surrogate error exceeds the adopted tolerances, the new FEM result is added to the dataset and the surrogate models are retrained. The proposed framework provides a scalable route for an efficient damage-aware optimization of seismic energy dissipation devices.

KEYWORDS
Buckling-delayed shear link, seismic energy dissipation, surrogate modelling, machine learning, radial basis functions, Differential Evolution, FEM validation, TFDMap

1 | INTRODUCTION

Shear-link beam (SLB) dampers are passive energy dissipation devices widely used in seismic-resistant structures, designed to undergo stable inelastic deformations while limiting damage to the primary system. Their configuration concentrates inelastic demand in replaceable components, enabling high energy dissipation, ductile response and stable hysteretic behavior under severe cyclic loading[1,2]. Within this family, buckling-delayed shear-link (BDSL) dampers incorporate a mechanical configuration that promotes shear-dominated behaviour while delaying local and global buckling.

The global hysteretic response of BDSL dampers can be characterized through experimental testing. However, laboratory campaigns present important limitations when addressing design optimization problems: internal state variables such as local plastic strains, stress triaxiality or damage indicators cannot be directly measured and the high cost and logistical complexity of

experimental programs restrict the number of geometric configurations that can be explored. These limitations become even more critical when the design objective is not only to increase global energy dissipation but also to control where and how damage develops within the device, making systematic optimization impractical.

In this context, finite element method (FEM) simulations provide a powerful framework for generating high-fidelity datasets across a wide range of geometric configurations, making them an ideal foundation for surrogate-based optimization strategies. Advanced nonlinear FEM models can accurately reproduce experimental cyclic behaviour, including plasticity, geometric nonlinearity, contact interactions, local instability and damage evolution, while providing access to both global response quantities and local indicators governing failure mechanisms. However, their high computational cost makes their direct use within optimization loops inefficient. This limitation motivates the use of surrogate models trained on FEM-generated data, which can approximate the structural response with reduced computational effort. The use of surrogate models enables the possibility of evaluating a large number of design configurations, facilitating systematic optimization.

Over the past decades, FEM has been widely used to study BDSL dampers and other passive seismic energy dissipation devices, providing detailed insight into nonlinear cyclic response, stiffness degradation and local inelastic mechanisms[3,4]. It has also supported the optimization and parametric analysis of these devices by enabling systematic exploration of geometric configurations and performance criteria under prescribed loading[5,6]. In this context, FEM-based studies have been extensively applied to characterize the mechanical response of metallic dampers. Motamedi et al.[7] investigated accordion metallic dampers through combined experimental and numerical analyses, assessing the influence of key geometric variables on stiffness, strength and energy dissipation. Ghamari et al.[8] studied I-shaped shear links in concentrically braced frames, while Xiong et al.[9] examined replaceable steel shear links with different short-length ratios, highlighting the strong influence of geometry on cyclic performance and failure modes. Simplified analytical and semi-empirical models have also been proposed to reduce computational cost[10] and more recent simulation-based studies have further explored the role of geometric and material variables in damper performance[11].

Geometric optimization has also been extensively explored. Zhang et al.[12] proposed a Kriging-assisted framework to maximize hysteretic energy in coupling beam dampers. Farzampour et al.[13] optimized butterfly-shaped shear links by maximizing the ratio between dissipated energy and plastic strain, while Khatibinia et al.[14,15] developed efficient strategies for U-shaped dampers using FEM and surrogate models. Shi et al.[16] introduced a non-parametric shape optimization framework for shear panel dampers and Saleh et al.[17,18] extended this line through topology optimization of shear-link configurations. More recent contributions include the hybrid cellular automata approach by Mendoza-Cuy et al.[19] and the statistical optimization framework by Rios et al.[20].

Data-driven approaches have mainly focused on response or property prediction. Chan et al.[21] used nonlinear autoregressive exogenous (NARX) models to reproduce hysteretic behaviour. Bae et al.[22] developed models for low-cycle fatigue estimation and Almasabha et al.[23] predicted the shear strength of short steel links using ML. Elgammal et al.[24] modelled hysteretic restoring forces using data-driven approaches, while Hu et al.[25] proposed explainable ML models for the probabilistic prediction of buckling stress. Physics-informed approaches have also been explored, such as the PINN framework proposed by Hu et al.[26].

All these works demonstrate the increasing interest in applying FEM-based and data-driven approaches, as well as in combining both, to analyse, understand and optimize seismic energy dissipation devices. However, most of these studies focus either on the prediction of the hysteretic response or on maximizing energy dissipation, leaving a critical aspect insufficiently explored: the need to control local damage while maintaining adequate dissipative capacity. In practice, excessive local damage may compromise structural integrity, reduce durability and lead to premature failure, even when global energy dissipation is improved.

The present work addresses this gap through a damage-aware surrogate-assisted optimization methodology in which the objective is not only to maximize distortion or energy dissipation, but also to balance dissipative performance with damage indicators derived from FEM simulations. The proposed approach combines: (i) experimentally calibrated nonlinear FEM models used as numerical ground truth; (ii) supervised surrogate models trained to predict local damage and distortion indicators; (iii) a Differential Evolution (DE) optimizer; and (iv) an adaptive FEM validation and retraining loop.

Figure 1 summarizes the proposed workflow. The different stages of the methodology, together with the surrogate modelling, optimization strategy, validation procedure, and corresponding results, are described in the following sections.

2 | BUCKLING-DELAYED SHEAR-LINK DAMPER

The BDSL dampers analysed in this work, with one representative configuration shown in Figure 2, are designed to concentrate energy dissipation in localized reduced-thickness zones, hereafter referred to as *windows*, while maintaining the overall structural integrity of the device. The dissipative element is connected to a surrounding load-transfer system through a mechanism

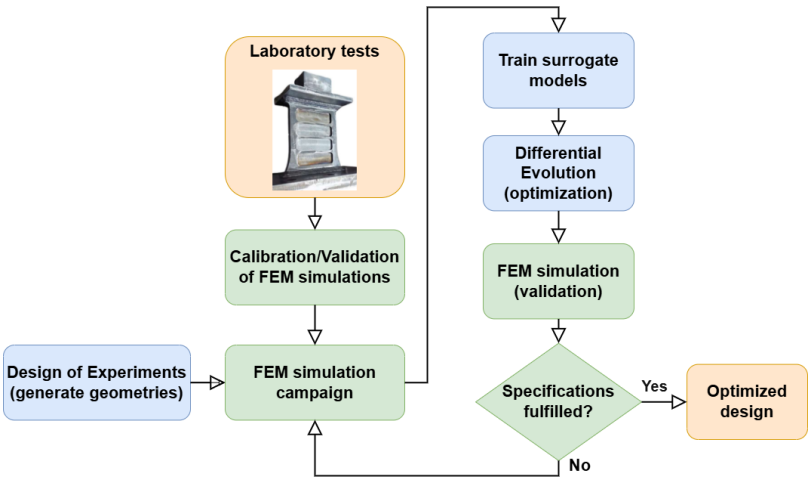

FIGURE 1 Flow chart of the proposed adaptive surrogate-assisted optimization framework.

that allows imposed in-plane displacement while preventing axial force transmission, thereby promoting a shear-dominated response. Under cyclic loading, the windows are intended to concentrate plastic deformation and dissipative demand, whereas the surrounding frame provides load transfer, stability and confinement without becoming the primary source of dissipation.

FIGURE 2 Representative BDSL damper configuration analysed in this work. The optimization variables correspond to the window thicknesses, while the surrounding frame dimensions remain fixed. Replace figure with a version including geometric dimensions.

This separation of functions leads to a non-trivial design problem. Thin windows may enhance ductility and dissipative activation, but they may also promote excessive damage localization. Conversely, thicker windows may increase strength while transferring inelastic demand to the frame. Since severe frame damage may compromise the structural integrity of the device, frame damage must be penalized more strongly than window damage. In addition, the dissipative demand should be distributed as uniformly as possible among the windows, avoiding configurations in which a single window absorbs most of the deformation while the remaining windows remain underused.

The dissipation mechanism is governed by controlled yielding of the windows under cyclic shear deformation. However, the interaction between shear deformation in the windows and bending or longitudinal effects in the frame leads to non-uniform damage distributions. Consequently, the design problem cannot be reduced to maximizing force or total dissipated energy alone. It must also explicitly control where damage develops and ensure a balanced participation of all windows in the dissipative process.

The design variables considered in this work are the window thicknesses

$$\mathbf{x} = \left[t_{w,1}, t_{w,2}, \ldots, t_{w,W}\right], \tag{1}$$

where W denotes the number of windows. The width and height identifiers of the device are represented by B and H, respectively. Three geometry families are considered in the current implementation: two-window devices with $H = 30$ cm, three-window devices with $H = 45$ cm, and five-window devices with $H = 60$ cm. For the two-window and three-window families, two different widths are analysed, namely $B = 29$ cm and $B = 34$ cm, whereas the five-window family is currently implemented only for a single width configuration $B = 34$ cm.

The admissible thickness ranges are defined according to the geometry family and manufacturing constraints. The corresponding bounds for each design variable are summarized in Table 1. In all cases, the frame thickness is kept constant at 30 mm.

Revisar las medidas no me ha equivocado.

TABLE 1 Geometry families and surrogate input variables considered in the current implementation.

Family	Height H	Width B	Frame thickness	Design variables	Thickness bounds
2 windows	30 cm	29/34 cm	30 mm	$t_{w,1}, t_{w,2}$	10–20 mm
3 windows	45 cm	29/34 cm	30 mm	$t_{w,1}, t_{w,2}, t_{w,3}$	5–14 mm
5 windows	60 cm	34 cm	30 mm	$t_{w,1}, \ldots, t_{w,5}$	5–12 mm

3 | FEM-CALIBRATED NUMERICAL GROUND TRUTH

3.1 | Nonlinear FEM model

El material es acero ASTM A36, ¿no? Estaría bien poner una referncia al software utilizado para los cálculos FEM

The surrogate models are trained using data generated from three-dimensional FEM simulations, as shown in Figure 3. The numerical model is based on a previously calibrated representation of the BDSL device. The steel dissipator is modelled using ASTM A36 steel, with cyclic plasticity described by the Yoshida–Uemori model[27,28]. The formulation accounts for both material and geometric nonlinearities, as well as contact interactions and boundary conditions consistent with the experimental setup. The steel component is discretized using linear eight-node hexahedral elements, providing a structured three-dimensional representation suitable for extracting local stress and strain fields.

The imposed displacement is applied through an actuator-like connector that transfers horizontal displacement while preventing axial load transmission. Additional contact and confinement conditions are included to reproduce the experimental anti-buckling configuration. The cyclic loading protocol is displacement-controlled and follows progressively increasing amplitudes, consistent with standard experimental qualification procedures for seismic energy dissipation devices.

Faltan por meter los ciclos de carga aplicados para cada geometría.

3.2 | Calibration and validation

¿Tenemos alguna publicación que podamos citar sobre la calibración de los modelos FEM?

The FEM model is calibrated against experimental cyclic tests. The calibration procedure involves the definition of the material model, the assembled geometry, as well as the contact and boundary conditions. The validated model accurately reproduces the main global experimental responses, including hysteretic force–displacement loops, cumulative dissipated energy and the corresponding skeleton curve.

Once validated, the numerical model is used as a reliable ground truth to evaluate configurations beyond those experimentally tested. Figure 4 presents the comparison between experimental and numerical results, showing good agreement in terms of global response and energy dissipation.

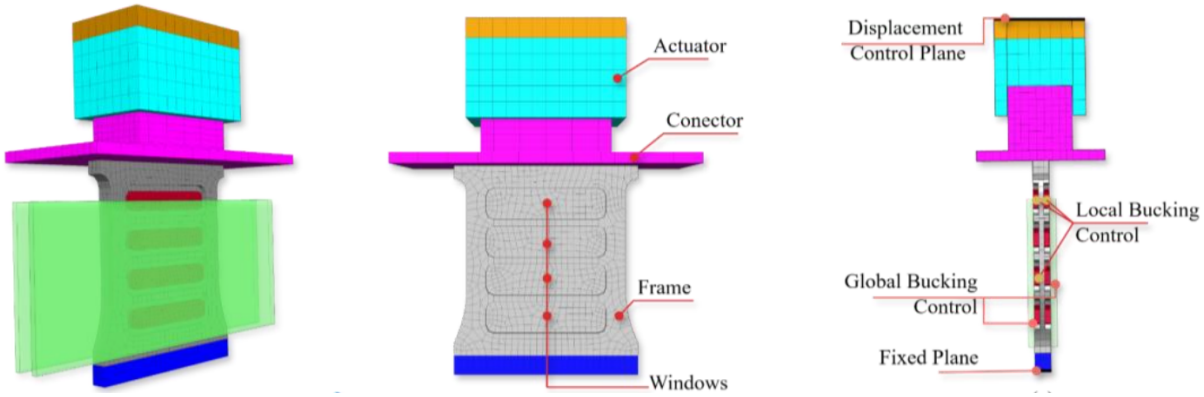

FIGURE 3 Finite element model used to generate the ground-truth dataset. The calibrated model reproduces the experimental cyclic response and provides internal quantities not directly accessible from laboratory tests. The image shows the mesh discretization, main components and boundary conditions, including local and global buckling control. ¿Tenemos una imagen de uno de los disipadores que se usan en este estudio?

The calibrated FEM model is subsequently employed to generate the datasets used for surrogate training and optimization, providing access to local damage and distortion indicators that cannot be directly measured in experiments.

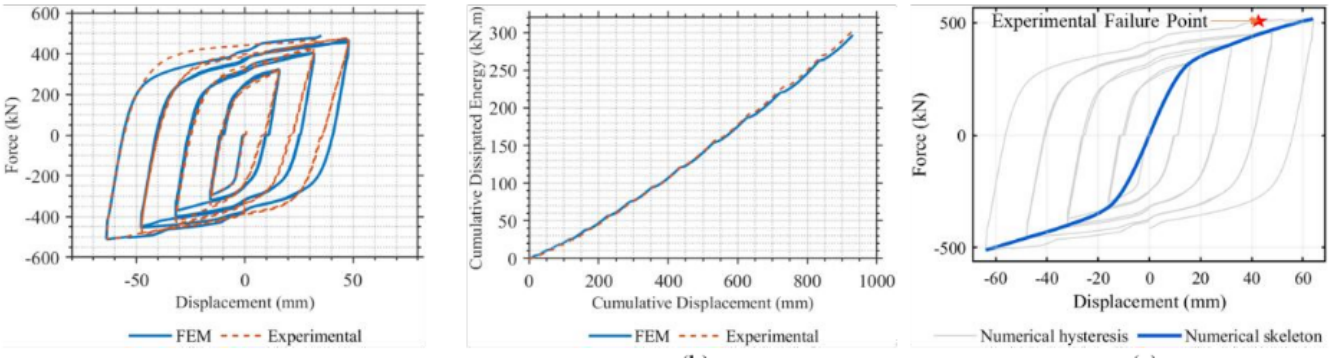

FIGURE 4 Experimental–numerical validation of the BDSL model. Comparison of hysteretic response, cumulative dissipated energy and skeleton curve, showing good agreement between FEM predictions and experimental results. ¿Tenemos una imagen de uno de los disipadores que se usan en este estudio?

3.3 | Damage and deformation indicators

The optimization strategy proposed in this work requires internal response variables that cannot be directly measured experimentally, making FEM simulations an appropriate source of data. These variables include local damage indicators in both the dissipative windows and the surrounding frame, as well as the distribution of deformation among the different regions of the device.

Among the available damage measures, stress-triaxiality-based indicators provide a meaningful description of ductile damage under multiaxial loading conditions. In this study, the Triaxial Failure Damage Map (TFDMap)[29] is adopted as a post-processing indicator to evaluate the proximity to ductile failure[30,31,32,33]. The TFDMap is obtained by comparing the local stress state, characterized by the stress triaxiality, together with the accumulated equivalent plastic strain, against a reference failure envelope. During cyclic loading, each material point evolves through a trajectory in the triaxiality–strain space, and the associated TFDMap value provides a quantitative measure of proximity to ductile fracture.

In the present work, the TFDMap is not employed as a constitutive fracture criterion, but rather as a robust damage-screening indicator suitable for comparing different geometrical configurations in terms of their relative proximity to failure. The objective is therefore not to predict crack initiation explicitly, but to ensure that the optimized configurations remain within acceptable damage levels while maintaining adequate dissipative performance.

For optimization purposes, damage is evaluated separately in the dissipative windows and in the surrounding frame. The damage index is computed using the average TFDMap value of the 12 nodes with the highest values within each region. This approach captures the most critical damage levels while avoiding excessive sensitivity to isolated local peaks. The resulting damage indicator associated with each window is denoted by TFDMap_i, whereas the corresponding value in the frame is represented by TFDMap_f.

In addition, the maximum local shear distortion in each window is denoted by $\varepsilon_{xy,i}$. This quantity is used as a proxy for dissipative activation, since larger stable distortions are generally associated with higher energy dissipation capacity. The contribution of each window is weighted depending on its geometric volume, ensuring that the evaluation accounts not only for point-wise strain values but also for the effective material volume involved in the dissipation process.

4 | DATASET GENERATION AND SURROGATE MODELLING

4.1 | Design of experiments

The FEM campaign is designed to cover the admissible design domain of each device family. Latin Hypercube Sampling (LHS) is used to generate a homogeneous set of thickness combinations within the prescribed bounds. This sampling strategy is well suited to the current problem because each window thickness has a bounded interval and the number of design variables increases with the number of windows. The FEM results stored: the input variables $t_{w,i}$ and the target outputs, including $\varepsilon_{xy,i}$, TFDMap_i and TFDMap_f.

The training process is iterative. For each configuration family, the first optimization iteration starts from an initial number of FEM rows. In the current implementation, the starting number of rows is 8 for two-window devices, 16 for three-window devices and 64 for five-window devices. Additional FEM simulations can be appended in subsequent iterations when the optimized design does not satisfy the validation criteria.

4.2 | Supervised ML surrogate models

In contrast to previous works focused on a single model or performance metric, this study provides a systematic comparison of surrogate techniques in terms of predictive accuracy and computational cost within the context of geometry optimization. The supervised surrogate set includes Random Forest (RF), Gradient Boosting Regression (GBR), XGBoost, Support Vector Regression (SVR), Multilayer Perceptron (MLP) and Gaussian Process Regression (GPR). Since preliminary calculations indicated that SVR and GPR often dominate the high-accuracy regime, RBF interpolants are also assessed as a computationally efficient alternative for fast optimization. The novelty is not the development of a new constitutive model, but the integration of FEM-calibrated damage indicators into an optimization workflow that explicitly distinguishes between damage in the windows and damage in the frame, encourages balanced window activation and verifies the optimized geometry with a high-fidelity FEM simulation before accepting it.

A set of supervised regression models is trained independently for each output variable. The considered algorithms are RF, GBR, XGBoost, SVR, MLP and GPR. The input vector is composed only of the window thicknesses of the corresponding device family. For each output, the model-selection routine evaluates all candidate algorithms and stores the best model as a serialized `joblib` file.

Hyperparameters are optimized using Bayesian search with 40 iterations. The scoring metrics are root mean squared error (RMSE), mean absolute error (MAE) and R^2. Since the available dataset size changes between geometry families and between adaptive iterations, the cross-validation strategy is selected automatically. Leave-One-Out validation is used for datasets with $N \leq 20$, repeated five-fold cross-validation with five repetitions is used for $21 \leq N \leq 80$ and standard shuffled five-fold cross-validation is used for larger datasets. For small datasets, the hyperparameter search spaces of tree-based models are reduced to mitigate overfitting.

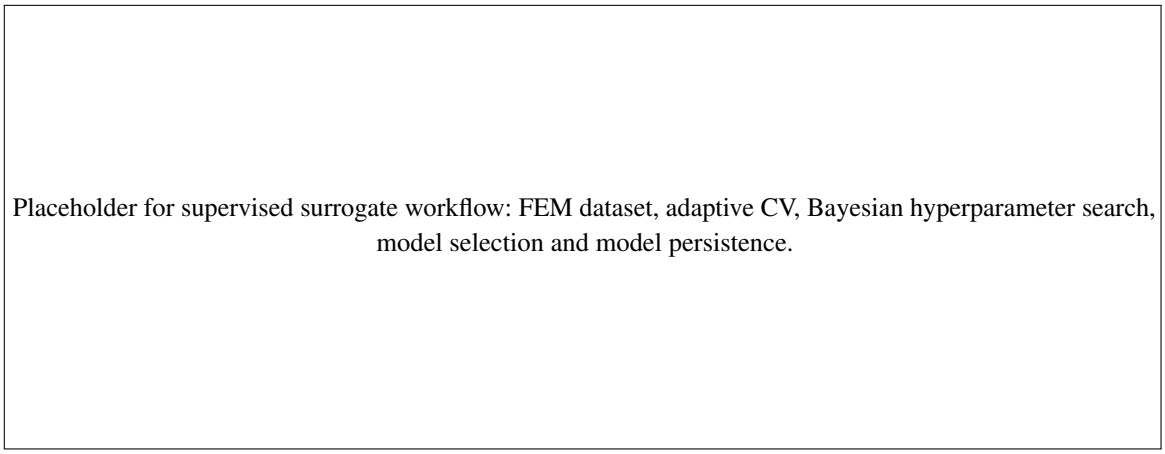

FIGURE 5 Supervised surrogate training workflow. A separate model is trained for each damage or distortion output. The selected model can differ from one output to another.

The best model is not selected exclusively from the lowest mean RMSE. Models whose RMSE lies within a 5% band from the best RMSE are considered competitive; when the dispersion of fold-level RMSE is available for all competitive candidates, the model with the lowest coefficient of variation of RMSE is selected. This criterion favours not only accurate but also stable surrogates, which is relevant in optimization because a small local error near an active damage constraint can change the accepted geometry.

Preliminary executions of this workflow indicate that SVR and GPR frequently provide the best accuracy for the considered datasets. This observation motivated the additional assessment of RBF interpolation as a simpler and faster surrogate strategy, especially for low-dimensional or well-sampled design spaces.

4.3 | RBF surrogate models

The RBF surrogate is implemented as a wrapper around the `scipy.interpolate.Rbf` interpolator. For each output variable, the model is trained using the same input features as the supervised ML surrogates. The current implementation uses a multiquadric radial basis function with zero smoothing and automatic shape parameter selection. The prediction model can be written generically as

$$\hat{y}(\mathbf{x}) = \sum_{j=1}^{N} \lambda_j \, \phi\left(\|\mathbf{x} - \mathbf{x}_j\|\right), \tag{2}$$

where $\mathbf{x}_j$ are the FEM-sampled geometries, λ_j are interpolation weights and ϕ is the selected radial basis function.

RBF models are evaluated through Leave-One-Out validation. For each output, the procedure repeatedly removes one FEM sample, trains the RBF interpolant with the remaining samples, predicts the left-out sample and computes RMSE, MAE, R^2 and dispersion metrics. This validation is especially useful because the number of FEM simulations is limited and because interpolation accuracy may be sensitive to the local density of training samples.

5 | DAMAGE-AWARE SURROGATE-ASSISTED OPTIMIZATION

5.1 | Optimization algorithm

The geometric optimization is carried out with Differential Evolution. DE is a population-based global optimizer that does not require gradient information and is therefore suitable for nonlinear, non-convex surrogate response surfaces. In the current implementation, the DE algorithm is run with a maximum of 500 iterations, a population size factor of 25, a convergence tolerance of 10^{-6} and a fixed random seed equal to 42 for reproducibility.

For each candidate geometry $\mathbf{x}$, the trained surrogate models predict the window distortions $\hat{\varepsilon_{xy}}_i$, the window damage indicators $\widehat{\text{TFDMap}}_i$ and the frame damage indicator $\widehat{\text{TFDMap}}_f$. These predictions are then combined into a scalar objective function to be minimized.

5.2 | Objective function

The objective function is designed to encode four mechanical rules:

1. the damage indicator must remain limited in all structural components, including both windows and frame;
2. reaching complete or near-complete damage in the frame is much more critical than reaching a similar damage level in a window, because frame failure would imply loss of the structural integrity of the damper;
3. the windows should develop comparable damage levels so that the dissipation mechanism is distributed rather than concentrated in a single window;
4. if several geometries show similar damage performance, the preferred one is the geometry that dissipates more energy, approximated through stable window distortion and the corresponding volume contribution.

The implemented scalar objective is

$$J(\mathbf{x}) = -\sum_{i=1}^{W} \hat{\varepsilon_{xy}}_i^{\,2}\, t_{w,i}\, V_i + \sum_{i=1}^{W} P_w\left(\widehat{\text{TFDMap}}_i; \text{TFDMap}_w^{\star}\right) + P_f\left(\widehat{\text{TFDMap}}_f; \text{TFDMap}_f^{\max}\right), \tag{3}$$

where V_i is the volume factor associated with window i, $\text{TFDMap}_w^{\star}$ is the target TFDMap level for the windows and $\text{TFDMap}_f^{\max}$ is the maximum admissible frame threshold. The first term is negative because the optimizer minimizes J; therefore, larger distortion contributions reduce the objective value.

The window penalty is defined as

$$P_w\left(\widehat{\text{TFDMap}}_i; \text{TFDMap}_w^{\star}\right) = \begin{cases} \left(\widehat{\text{TFDMap}}_i - \text{TFDMap}_w^{\star}\right)^2, & \widehat{\text{TFDMap}}_i > \text{TFDMap}_w^{\star}, \\ \left|\widehat{\text{TFDMap}}_i - \text{TFDMap}_w^{\star}\right|, & \widehat{\text{TFDMap}}_i \le \text{TFDMap}_w^{\star}. \end{cases} \tag{4}$$

This expression penalizes exceeding the target value quadratically, while also discouraging excessively under-utilized windows through a linear distance to the target. As a result, the optimizer tends to equalize the TFDMap levels among windows rather than forcing all windows to remain far below the admissible damage level.

The frame penalty is more severe:

$$P_f\left(\widehat{\text{TFDMap}}_f; \text{TFDMap}_f^{\max}\right) = \begin{cases} \left(\widehat{\text{TFDMap}}_f - \text{TFDMap}_f^{\max}\right)^3, & \widehat{\text{TFDMap}}_f > \text{TFDMap}_f^{\max}, \\ 0, & \widehat{\text{TFDMap}}_f \le \text{TFDMap}_f^{\max}. \end{cases} \tag{5}$$

The cubic frame penalty reflects the fact that complete frame failure is a much more severe event than localized damage in a replaceable window. In the current scripts, $\text{TFDMap}_f^{\max} = 90$ is used, while the target window threshold $\text{TFDMap}_w^{\star}$ is provided as an input argument to the optimizer.

5.3 | Volume factors

The distortion contribution is weighted by a geometric factor that accounts for the effective volume associated with each window. These factors differ between families because the windows have different dimensions and positions. The current values used in the scripts are summarized in Table 2. When a geometry family is not explicitly covered, the implementation falls back to an unweighted contribution.

TABLE 2 Window volume factors used to weight the distortion contribution in the objective function.

Family	Width identifier B	Volume factors V_i
2 windows	29	0.0208, 0.0185
2 windows	34	0.0263, 0.0240
3 windows	29	0.0229, 0.0210, 0.0185
3 windows	34	0.0262, 0.0262, 0.0240
5 windows	–	0.0410, 0.0265, 0.0240, 0.0098, 0.0098

6 | ADAPTIVE FEM VALIDATION AND RETRAINING

The adaptive validation stage is a central component of the proposed framework. Once an optimal geometry is identified by the surrogate-assisted optimizer, it is re-evaluated with FEM to verify that the surrogate remains accurate in the region of the design space where the optimum lies. The candidate geometry is accepted only if: (i) the prediction error of all damage and distortion variables remains below the prescribed tolerance; (ii) the absolute error of the objective function remains within the admissible limit; and (iii) the optimized window thicknesses remain stable between consecutive optimization iterations, with variations smaller than a prescribed percentage of the full design range. If any of these criteria is not satisfied, the new FEM result is incorporated into the training dataset and the surrogate models are retrained.

As a result, the main contribution of this work lies in the development of a robust, scalable and physically informed design methodology that explicitly accounts for the trade-off between energy dissipation and damage. To summarize, the main contributions of this work are:

- generation of high-fidelity FEM datasets for BDSL dampers with increasing geometric complexity and different numbers of dissipative windows;
- geometric optimization using surrogate models, including supervised ML techniques and RBF interpolants;
- systematic comparison of surrogate strategies in terms of predictive accuracy, computational cost and practical suitability for optimization;
- a damage-aware objective function that combines window damage control, severe frame-damage penalization, window-to-window damage balancing and dissipated-energy maximization;
- an adaptive FEM validation and retraining strategy based on explicit tolerances for surrogate error, objective-function error and stability of the optimized geometry between successive iterations.

The surrogate-optimized geometry is not accepted directly. Instead, the optimal candidate proposed by the surrogate-assisted DE process is evaluated with the high-fidelity FEM model. This validation step checks whether the surrogate has remained reliable in the region of the design space selected by the optimizer.

Three acceptance criteria are used. First, the prediction error of all variables entering the optimization process, including damage and distortion indicators, must be lower than 5%. Second, the absolute error in the objective function must be lower than 10. Third, the optimized window thicknesses must be stable between consecutive optimization iterations: no thickness is allowed to change by more than 2% of the total admissible range. For example, if a thickness is optimized within the interval 10–20 mm, the total range is 10 mm and the maximum admissible variation between iterations is 0.2 mm.

If all criteria are satisfied, the FEM-validated geometry is accepted as the optimized design. If at least one criterion is not satisfied, the new FEM result is added to the dataset, the surrogate models are retrained and the DE optimization is repeated. This loop is summarized in Figure 6. The process reduces the risk of accepting a geometry that is optimal only because of surrogate extrapolation error.

7 | PLANNED NUMERICAL ASSESSMENT

The full numerical results are currently being generated. This section is therefore structured as the target results section to be completed once the final training, optimization and FEM-validation outputs are available. The tables and figures indicated below should be filled with the final values obtained from the scripts.

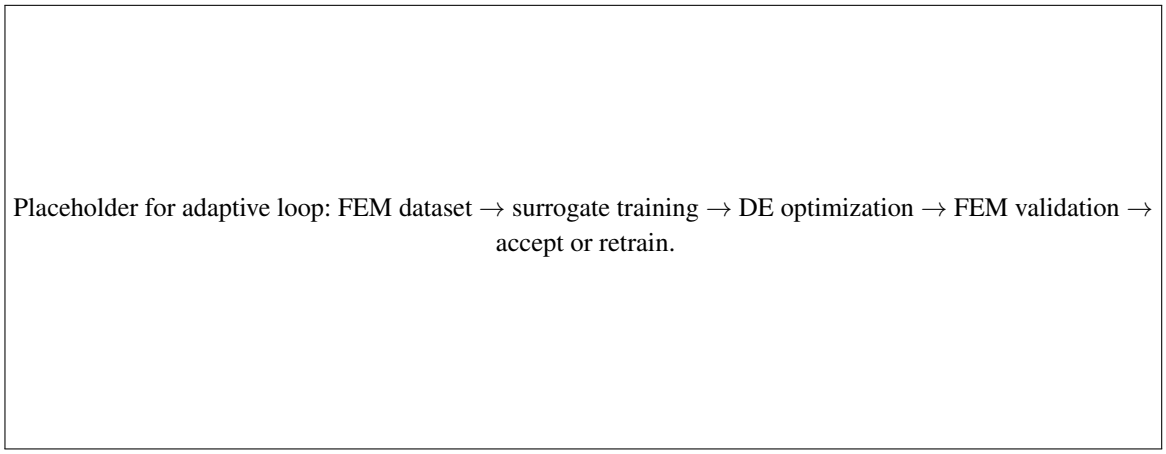

FIGURE 6 Adaptive FEM validation and retraining loop. The optimized geometry is accepted only when prediction errors, objective error and geometry stability criteria are simultaneously satisfied.

TABLE 3 Template for reporting the supervised surrogate performance. Replace placeholders with the final results obtained from the training scripts.

Family	Output	Best model	RMSE	MAE	R^2	Training time [s]
2W–B29–H30	$\varepsilon_{xy,1}$	[SVR/GPR/etc.]	[–]	[–]	[–]	[–]
2W–B29–H30	TFDMap_1	[SVR/GPR/etc.]	[–]	[–]	[–]	[–]
2W–B29–H30	TFDMap_f	[SVR/GPR/etc.]	[–]	[–]	[–]	[–]
3W–B34–H45	$\varepsilon_{xy,i}$	[SVR/GPR/etc.]	[–]	[–]	[–]	[–]
5W–H60	TFDMap_i	[SVR/GPR/etc.]	[–]	[–]	[–]	[–]

TABLE 4 Template for comparing supervised ML and RBF surrogates.

Family	Output	Best supervised model	Supervised RMSE	RBF LOO RMSE	Relative speed-up
2W–B29–H30	$\varepsilon_{xy,1}$	[–]	[–]	[–]	[–]
2W–B29–H30	TFDMap_1	[–]	[–]	[–]	[–]
3W–B34–H45	TFDMap_f	[–]	[–]	[–]	[–]
5W–H60	$\varepsilon_{xy,i}$	[–]	[–]	[–]	[–]

7.1 | Predictive performance of supervised ML models

For each device family and each adaptive iteration, the supervised training script produces two CSV files: a summary table containing the selected model for each output and a detailed table containing the performance of every candidate model. The final paper should report RMSE, MAE, R^2, training time and selected hyperparameters for the relevant outputs. Special attention should be paid to the variables entering the objective function: $\varepsilon_{xy,i}$, TFDMap_i and TFDMap_f.

Based on preliminary tests, it is expected that SVR and GPR will be among the most accurate models for several target variables. This should be confirmed quantitatively using the final cross-validation summaries.

7.2 | RBF validation and computational efficiency

The RBF training script performs Leave-One-Out validation for each output and stores RMSE, MAE, R^2 and error-dispersion indicators. The comparison with supervised ML models should be presented in terms of both predictive accuracy and computational efficiency. RBF models are expected to be particularly competitive when the design space is low-dimensional and the FEM samples cover the domain adequately.

TABLE 5 Template for reporting optimized geometries and FEM validation.

Family	Surrogate	$\mathrm{TFDMap}_w^\star$	$t_{w,1}$	$t_{w,2}$	$t_{w,3}$	$\max(\mathrm{TFDMap}_f)$ FEM	Accepted?
2W–B29–H30	ML	80	[–]	[–]	–	[–]	[yes/no]
2W–B29–H30	RBF	80	[–]	[–]	–	[–]	[yes/no]
3W–B34–H45	ML	90	[–]	[–]	[–]	[–]	[yes/no]
3W–B34–H45	RBF	90	[–]	[–]	[–]	[–]	[yes/no]

Placeholder for final optimization results: predicted vs FEM TFDMap_i, TFDMap_f, $\varepsilon_{xy,i}$ and objective value for ML and RBF surrogates.

FIGURE 7 Recommended final validation plot comparing surrogate predictions and FEM results for the optimized geometries.

7.3 | Optimization results

For each surrogate type, device family, width identifier, window threshold and adaptive iteration, the optimization scripts export a CSV file containing the optimal thicknesses, objective value, predicted distortions, predicted window TFDMap values and predicted frame TFDMap. These results should be compared with the corresponding FEM validation values.

The expected interpretation is that the optimized designs should approach the target window TFDMap level while keeping the frame below its admissible threshold. A successful optimization should also avoid concentrating almost all damage in a single window. Therefore, figures showing the window-to-window distribution of TFDMap_i and $\varepsilon_{xy,i}$ are recommended.

8 | DISCUSSION

The proposed methodology addresses a central limitation of direct FEM-based damper optimization: the high cost of evaluating many nonlinear cyclic simulations. By training surrogate models on FEM-calibrated datasets, the optimizer can explore the design domain efficiently while retaining a connection to the underlying mechanics of the device. The adaptive validation loop is essential because it prevents the optimizer from relying blindly on surrogate predictions in regions where the training data may be sparse.

The objective function also reflects the mechanical hierarchy of the BDSL device. Damage in the windows is not intrinsically undesirable; it is the intended mechanism for energy dissipation, provided that it remains below the adopted threshold and is reasonably distributed among windows. By contrast, damage in the frame is structurally more critical. The cubic frame penalty therefore gives the optimizer a clear preference for geometries that keep the frame safe, even if another geometry could dissipate slightly more energy. This is consistent with the design philosophy of replaceable dissipative devices, where controlled damage should be localized in predefined sacrificial regions.

The inclusion of RBF models is motivated by practical computational considerations. Supervised models such as SVR and GPR may provide high predictive accuracy, but they require hyperparameter optimization and cross-validation. RBF models, in contrast, can be trained with minimal overhead and can provide very fast predictions. Their performance is expected to depend

strongly on the dimensionality of the design space and on the density of FEM sampling. Therefore, the final comparison should not identify a universally best surrogate, but rather establish when each surrogate class is preferable.

Some limitations should be highlighted. First, the methodology is only as reliable as the calibrated FEM model used to generate the data. Second, TFDMap is used as a damage indicator and not as a direct fracture model. Third, the current optimization considers window thicknesses as design variables; additional variables such as window height, spacing, frame thickness or filler properties could be incorporated in future work but would require a larger FEM dataset. Finally, the optimized geometries should ultimately be validated experimentally before being used for design recommendations.

9 | CONCLUSIONS

This work presents an adaptive surrogate-assisted optimization framework for BDSL dampers under cyclic seismic loading. The methodology combines FEM-calibrated numerical simulations, supervised ML models, RBF interpolation, Differential Evolution and FEM-based validation of the optimized geometries. The following conclusions can be drawn from the proposed formulation:

1. The BDSL optimization problem must be formulated as a damage-aware design problem rather than as a pure energy-maximization problem. The same energy level may correspond to different local damage distributions and different safety margins in the frame.
2. FEM simulations provide the necessary ground truth for training because they supply internal indicators such as TFDMap and local distortion, which cannot be obtained experimentally with the same spatial resolution.
3. Supervised ML models and RBF interpolants provide complementary surrogate strategies. SVR and GPR are expected to be highly accurate based on preliminary tests, while RBF models offer a faster alternative for well-sampled design domains.
4. The proposed objective function explicitly encodes the desired mechanical behaviour: controlled window damage, severe penalization of frame damage, balanced participation of windows and preference for higher dissipated energy when damage performance is comparable.
5. The adaptive FEM validation and retraining loop is a key component of the framework. A candidate geometry is accepted only if surrogate predictions match FEM results within the defined tolerances and if the optimized thicknesses remain stable between consecutive iterations.

Once the final numerical campaign is completed, the placeholders in Section 7 should be replaced by the final model-selection tables, RBF validation metrics, optimized geometries and FEM-validation comparisons.

AUTHOR CONTRIBUTIONS

[To be completed according to the final author list.] Conceptualization: J. Ramirez, J. Gonzalez, F. Rastellini, G. Bozzo, L. Bozzo, J. Irazabal. Methodology: J. Ramirez, J. Gonzalez, F. Rastellini, J. Irazabal. Software and surrogate optimization: J. Ramirez, J. Gonzalez, J. Irazabal. FEM modelling and validation: J. Ramirez, F. Rastellini, G. Bozzo, L. Bozzo. Writing–original draft: J. Ramirez and J. Irazabal. Writing–review and editing: all authors.

ACKNOWLEDGMENTS

The authors acknowledge the financial support of Project ACE100/23/000022, “Edificacions resilients equipades amb dissipadores Shear Link”, funded by the Government of Catalonia through ACCIO and with the support of the Catalan Office for Climate Change, with the participation of Luis Bozzo Estructuras y Proyectos S.L. and the Centre Internacional de Metodes Numerics en Enginyeria (CIMNE).

FINANCIAL DISCLOSURE

None reported.

CONFLICT OF INTEREST

The authors declare no potential conflict of interests.

REFERENCES

1. Malley JO, Popov EP. Shear Links in Eccentrically Braced Frames. *Journal of Structural Engineering.* 1984;110(9):2275–2295. doi: 10.1061/(ASCE)0733-9445(1984)110:9(2275)

2. Okazaki T, Engelhardt MD. Cyclic loading behavior of EBF links constructed of ASTM A992 steel. *Journal of Constructional Steel Research.* 2007;63(6):751–765. doi: 10.1016/j.jcsr.2006.08.004
3. Deng K, Pan P, Su Y, Ran T, Xue Y. Development of an energy dissipation restrainer for bridges using a steel shear panel. *Journal of Constructional Steel Research.* 2014;101:83–95. doi: 10.1016/j.jcsr.2014.03.009
4. Deng K, Pan P, Li W, Xue Y. Development of a buckling restrained shear panel damper. *Journal of Constructional Steel Research.* 2015;106:311–321. doi: 10.1016/j.jcsr.2015.01.004
5. Deng K, Pan P, Sun J, Liu J, Xue Y. Shape optimization design of steel shear panel dampers. *Journal of Constructional Steel Research.* 2014;99:187–193. doi: 10.1016/j.jcsr.2014.03.001
6. Deng K, Pan P, Su Y, Xue Y. Shape optimization of U-shaped damper for improving its bi-directional performance under cyclic loading. *Engineering Structures.* 2015;93:27–35. doi: 10.1016/j.engstruct.2015.03.006
7. Motamedi M, Nateghi-A. F. Study on mechanical characteristics of accordion metallic damper. *Journal of Constructional Steel Research.* 2018;142:68–77. doi: 10.1016/j.jcsr.2017.12.010
8. Ghamari A, Kim YJ, Bae J. Utilizing an I-shaped shear link as a damper to improve the behaviour of a concentrically braced frame. *Journal of Constructional Steel Research.* 2021;186:106915. doi: 10.1016/j.jcsr.2021.106915
9. Xiong L, Guo Z, Cai J, Jiang K, Li L. Seismic performance of the replaceable steel links with different short length ratios. *Sci Rep.* 2024;14(1):29976. doi: 10.1038/s41598-024-81336-8
10. Deng K, Pan P, Lam A, Xue Y. A simplified model for analysis of high-rise buildings equipped with hysteresis damped outriggers. *The Structural Design of Tall and Special Buildings.* 2014;23(15):1158–1170. _eprint: https://onlinelibrary.wiley.com/doi/pdf/10.1002/tal.1113doi: 10.1002/tal.1113
11. Kim YC, Mortazavi SJ, Farzampour A, Hu JW, Mansouri I, Awoyera PO. Optimization of the Curved Metal Damper to Improve Structural Energy Dissipation Capacity. *Buildings.* 2022;12(1):67. doi: 10.3390/buildings12010067
12. Zhang Z, Ou J, Li D, Zhang S. Optimization Design of Coupling Beam Metal Damper in Shear Wall Structures. *Applied Sciences.* 2017;7(2):137. doi: 10.3390/app7020137
13. Farzampour A, Khatibinia M, Mansouri I. Shape optimization of butterfly-shaped shear links using Grey Wolf algorithm. *Ingegneria Sismica.* 2019;36:27–41.
14. Khatibinia M, Jalaipour M, Gharehbaghi S. Shape optimization of U-shaped steel dampers subjected to cyclic loading using an efficient hybrid approach. *Engineering Structures.* 2019;197:108874. doi: 10.1016/j.engstruct.2019.02.005
15. Khatibinia M, Ahrari A, Gharehbaghi S, et al. An efficient approach for optimum shape design of steel shear panel dampers under cyclic loading. *Smart Structures and Systems.* 2021;27(3):547–557. doi: 10.12989/sss.2021.27.3.547
16. Shi JX, Kozono S, Shimoda M, Takino M, Wada D, Liu Y. Non-parametric shape design optimization of elastic-plastic shear panel dampers under cyclic loading. *Engineering Structures.* 2019;189:48–61. doi: 10.1016/j.engstruct.2019.03.049
17. Saleh YN, Mourad SA, Ibrahim AM. Topology optimization of vertical shear links in eccentrically braced frames. *Structures.* 2024;66:106821. doi: 10.1016/j.istruc.2024.106821
18. Saleh YN, Mourad SA, Salem HG, Ibrahim AM. Computational study on stiffened topology-optimized shear links for eccentrically braced frames. *Bull Earthquake Eng.* 2026. doi: 10.1007/s10518-026-02417-9
19. Mendoza-Cuy A, Begambre-Carrillo O, Villalba-Morales JD. Topology optimization of steel slotted dampers with the hybrid cellular automata technique. *Advances in Engineering Software.* 2025;206:103921. doi: 10.1016/j.advengsoft.2025.103921
20. Ríos I, Gómez Á, Romero F, et al. Computational Design of High-Performance U-Shaped Seismic Dampers Using Statistical Optimization. *Materials.* 2025;18(23):5403. doi: 10.3390/ma18235403
21. Chan RWK, Yuen JKK, Lee EWM, Arashpour M. Application of Nonlinear-Autoregressive-Exogenous model to predict the hysteretic behaviour of passive control systems. *Engineering Structures.* 2015;85:1–10. doi: 10.1016/j.engstruct.2014.12.007
22. Bae J, Lee CH, Park M, Alemayehu RW, Ryu J, Ju YK. Modified Low-Cycle Fatigue Estimation Using Machine Learning for Radius-Cut Coke-Shaped Metallic Damper Subjected to Cyclic Loading. *Int J Steel Struct.* 2020;20(6):1849–1858. doi: 10.1007/s13296-020-00377-7
23. Almasabha G, Alshboul O, Shehadeh A, Almuflih AS. Machine Learning Algorithm for Shear Strength Prediction of Short Links for Steel Buildings. *Buildings.* 2022;12(6):775. doi: 10.3390/buildings12060775
24. Elgammal A, Ali Y. A novel hysteretic restoring force model for shear link dampers: A machine learning approach. *Structures.* 2024;70:107848. doi: 10.1016/j.istruc.2024.107848
25. Hu S, Wang W, Lu Y. Explainable machine learning models for probabilistic buckling stress prediction of steel shear panel dampers. *Engineering Structures.* 2023;288:116235. doi: 10.1016/j.engstruct.2023.116235
26. Hu Y, Guo W, Long Y, Li S, Xu Z. Physics-informed deep neural networks for simulating S-shaped steel dampers. *Computers & Structures.* 2022;267:106798. doi: 10.1016/j.compstruc.2022.106798
27. Yoshida F, Uemori T. A model of large-strain cyclic plasticity describing the Bauschinger effect and workhardening stagnation. *International Journal of Plasticity.* 2002;18(5–6):661–686. doi: 10.1016/S0749-6419(01)00050-X
28. Jia LJ. Integration algorithm for a modified Yoshida–Uemori model to simulate cyclic plasticity in extremely large plastic strain ranges up to fracture. *Computers & Structures.* 2014;145:36–46. doi: 10.1016/j.compstruc.2014.08.010
29. Rastellini F, Socorro G, Forgas A, Oñate E. A Triaxial Failure Diagram to predict the forming limit of 3D sheet metal parts subjected to multiaxial stresses. *J. Phys.: Conf. Ser.*. 2016;734(3):032020. doi: 10.1088/1742-6596/734/3/032020
30. Rice JR, Tracey DM. On the ductile enlargement of voids in triaxial stress fields. *Journal of the Mechanics and Physics of Solids.* 1969;17(3):201–217. doi: 10.1016/0022-5096(69)90033-7
31. Bao Y, Wierzbicki T. On fracture locus in the equivalent strain and stress triaxiality space. *International Journal of Mechanical Sciences.* 2004;46(1):81–98. doi: 10.1016/j.ijmecsci.2004.02.006
32. Wierzbicki T, Bao Y, Lee YW, Bai Y. Calibration and evaluation of seven fracture models. *International Journal of Mechanical Sciences.* 2005;47(4):719–743. doi: 10.1016/j.ijmecsci.2005.03.003
33. Bai Y, Wierzbicki T. A new model of metal plasticity and fracture with pressure and Lode dependence. *International Journal of Plasticity.* 2008;24(6):1071–1096. doi: 10.1016/j.ijplas.2007.09.004

SUPPORTING INFORMATION

Additional supporting information may include the FEM database, trained surrogate models, optimization scripts and final FEM-validation simulations.